MODELING OF RAREFIED HYPERSONIC FLOWS USING THE MASSIVELY PARALLEL DSMC KERNEL "SPARTA"

Angelos Klothakis[1], Ioannis K. Nikolos[2]

[1, 2] School of Production Engineering & Management, Technical University of Crete,
Chania, GR-73100, Greece.
e-mail: aklothakis@gmail.com, jnikolo@dpem.tuc.gr

Keywords: DSMC, external flows, hypersonic shocks.

Abstract. *This paper describes the application of a Direct Simulation Monte Carlo (DSMC) computational kernel, called SPARTA (Stochastic Parallel Rarefied-gas Time-accurate Analyzer) [1] to the capture of shock waves in rarefied hypersonic flows. Three cases are considered: a hypersonic flat plate simulation, a Mach 15.6 flow over a flared cylinder and a Mach 20.2 flow over a 70-degree planetary probe. For all three cases a comparison between experimental and numerical results is presented, to assess the ability of the code to effectively and efficiently simulate such demanding flows.*

1 INTRODUCTION

When the conditions of the flow are rarefied and hypersonic, a more suitable alternative to the use of Navier-Stokes equations for developing a numerical solution is the Direct Simulation Monte Carlo method (DSMC). The method was developed about 50 years ago by Graeme Bird [2] and now is a well-established technique for modelling low density gas flows. DSMC is a particle method, which employs a large number of particles in modelling a rarefied gas. In this paper the application of a new open-source DSMC computational kernel, called SPARTA (Stochastic PArallel Rarefied-gas Time-accurate Analyzer) is described [1]. Three cases are examined: a) a hypersonic flat plate simulation and comparison with DAC (DSMC Analysis Code) [3]; b) a Mach 20.2 flow over a 70-degree planetary probe; and c) a Mach 15.6 flow over a flared cylinder. Those test cases were selected in order to investigate the ability of the SPARTA open-source code in reproducing the fine features of the complicated flow phenomena connected with shock-boundary and shock-shock interactions, and its computational efficiency in a parallel computation environment. Moreover, additional objectives of this assessment procedure were the establishment of a "best-practice" for the construction of the computational grids around the examined bodies, and the gain of know-how on the optimal use of the open-source code.

The aforementioned test cases, along with their variants, have been previously used by other researchers to validate some of the very well-known parallel DSMC solvers, such as DAC, SMILE [4], MONACO [5], ICARUS [6], MGDS [7] and dsmcFoam [8]. For example, dsmcFoam solver, among other test cases, was also validated against the flow over the 70-degree blunt cone [9]. DAC solver, which is NASA's code for DSMC simulations, has been validated against a 25/65 degrees sharp cone [10]. Furthermore, MONACO has been tested on a flow over a blunt cone, along with other validation cases, such as a blunt cone at an angle of attack [11]. Some important characteristics of the flows developed around the test objects are very steep gradients of velocity, temperature and density, shock/shock interaction, compression and rapid expansion. Such features render the numerical simulation of these complex flows very demanding so that a special study on the simulation parameters (number of particles, grid density, time step, etc.) is needed.

For the flat plate test case, simulation experiments have been conducted in a free-jet expansion tunnel [12], forming a database to be used for code validation purposes. Regarding the planetary probe test case, its form was decided by the AGARD Group 18 [13], while the experimental results, to be used for code validation, can be found in [13, 14]. Regarding the flared cylinder case, a large number of experiments have been conducted in order to acquire accurate aero-thermodynamic results. The experiments were conducted on the SR3 wind tunnel, using nitrogen as the flow gas. The flared cylinder experiments, used in this study, were conducted at the Buffalo Research Center (CUBRC) wind tunnel [15]. This test case was selected because its shape has the ability to reproduce shock/shock and shock/boundary interactions.

2 THE DSMC METHODOLOGY

2.1 The DSMC algorithm

DSMC is a particle method based on the kinetic theory for the simulation of rarefied gases. The method models the gas flow by using many simulator particles, each representing a large number of real particles. In the DSMC method the time step (Δt) is chosen to be small enough so that the movement and collisions of the particles can be decoupled. During a DSMC simulation the flow field is discretized into computational cells, which provide geometric boundaries and volumes required to sample macroscopic properties. The algorithm has four main steps. Initially, given a time step Δt all particles move along their trajectories and interactions with boundaries are calculated. Then, all particles are indexed into cells, according to their positions. Subsequently, the collision pairs are selected and intermolecular collisions are performed on a probabilistic basis. Finally, flow properties such as velocity and temperature are obtained by sampling the microscopic state of particles in each cell. In figure 1 the DSMC algorithm flowchart is presented.

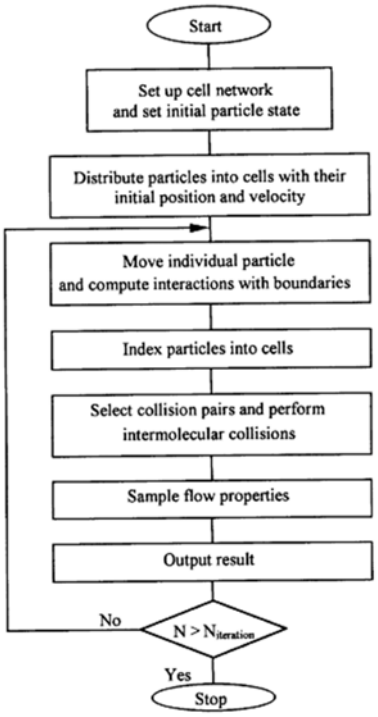

Figure 1. DSMC algorithm flowchart [2].

The computational approximations associated with the DSMC methodology are the ratio of the number of simulated molecules to the number of real molecules, the time step over which the molecular motion and collisions are decoupled, and the finite cell and sub-cell sizes in physical space. The fundamental requirements are that the linear dimensions of the cells should be small in comparison with the scale length of the macroscopic flow gradients in the stream-wise direction, which generally means that the cell dimensions should be of the order of the local mean free path, and the time step should be less than the local mean collision time. Theoretically, DSMC becomes more exact when the cell size and time step tend to zero [2].

2.2 Molecular models

Currently, in DSMC methodology four molecular models are used: The inverse power law model, the hard sphere model (HS), the variable hard sphere model (VHS), the variable soft sphere mode (VSS). In the cases simulated in this work, the variable sphere model is used. According to [2], there is a deficiency in the VHS model: the ratio of the momentum to the viscosity cross-section is constant and equal to $3/2$, while in the inverse power law model, which best approaches real gases, this ratio varies with the power law exponent. To alleviate this problem, the variable soft sphere model (VSS) was introduced; the only difference with the VHS model is that the deflection angle is given by

$$x = 2cos^{-1}(b/d)^{1/a}, \tag{1}$$

instead of:

$$x = 2cos^{-1}(b/d) \tag{2}$$

In eqn. (1) a is a coefficient between 1 and 2. Consequently, the viscosity and momentum transfer cross-sections become respectively:

$$\sigma_\mu = \frac{4a}{(a+1)(a+2)}\sigma_T \tag{3}$$

$$\sigma_M = \frac{2}{(a+1)}\sigma_T \tag{4}$$

According to [2] the VHS, VSS and inverse power law models lead to the same coefficient of viscosity, but only the VSS (contrary to the VHS one) leads to the same diffusion coefficient as the inverse power law model.

3 RESULTS AND DISCUSSION

3.1 Hypersonic flow over a flat plate

All simulations have been conducted on a DELL PowerEdge R815 system with 4 AMD™ Opteron™ 6380 16-core processors (64 cores in total) at 2.5 GHz, and 128GB RAM. In this first case DAC and SPARTA are compared against the rarefied flow around a rectangular flat-plate model within a free-jet expansion wind-tunnel; the geometry and flow conditions are described in [12]. This experiment is characterized by a rarefied global Knudsen number equal to 0.016, based on a free stream mean-free-path $\lambda = 1.6mm$ and a flat plate length equal to $L = 100mm$. Flat plate thickness is $5mm$. Moreover, in this simulation certain efficiency parameters are compared between DAC and SPARTA. The data for the DAC code were obtained from [16], while flow conditions are summarized in Table 1.

The computational grid used in this simulation is a two-dimensional structured grid with rectangular cells having 0.5 mm sides. The simulation domain is a symmetric orthogonal region around the flat-plate, with dimensions 180 mm by 205 mm in the *x*- and *y*-directions respectively. The inflow boundary is defined at the left side of the computational domain, while the outflow one is defined at the right side; reflective boundaries are used at the top and bottom sides. The flat plate solid boundary is defined by an interior region with dimensions 100 mm by 5 mm in the *x*- and *y*- directions respectively. The origin of the coordinate system was set at the center of the flat plate's left side. The entire flow field mesh was generated using level 1 cells. In order to determine the cell size, the rule of "one third of mean free path" was used; the free stream mean free path for the used flow conditions (Table 1) is 1.6 mm.

V_x (m/s)	T_∞ (K)	$n_\infty (m^{-3})$	T_w (K)	Time-step (s)
1504	13.32	3.716×10^{20}	290	3.102×10^{-7}

Table 1: Flat plate simulation flow conditions.

In this simulation free stream velocity is parallel to *x*-axis and to the longitudinal surfaces of the flat plate. The imposed flat plate boundary condition is that of an isothermal wall with wall temperature equal to $T_w = 290\ K$. Gas molecules are assumed to reflect diffusively from the wall, according to the Maxwellian distribution at T_w.

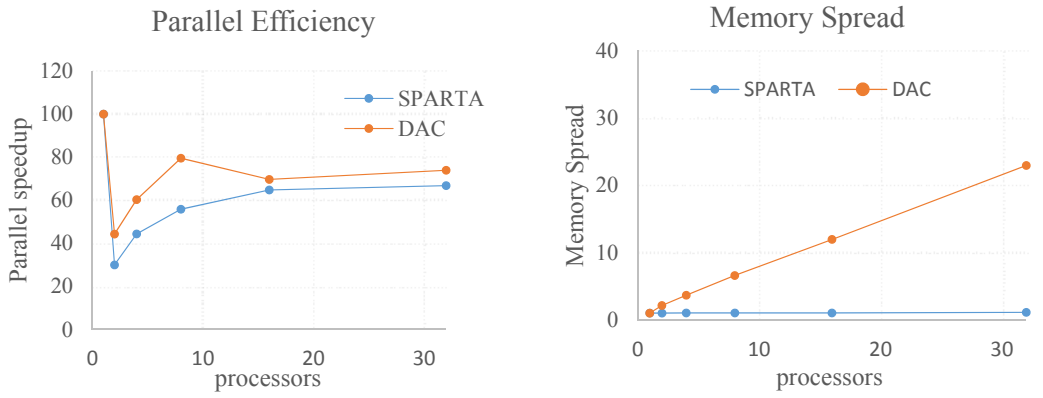

Figure 2. (Left) Parallel efficiency, (Right) Memory spread (flat plate test case).

In figure 2, two efficiency parameters, namely parallel efficiency and memory spread, are compared between the two codes. Parallel efficiency n_{ps} and memory spread s_{pm} are defined as:

$$n_{ps} = \frac{t_s}{N_{proc} \times t_{parallel}} \tag{5}$$

$$s_{pm} = \frac{\sum_{proc} m_{proc}}{m_s} \tag{6}$$

where t_s and $t_{parallel}$ are serial and parallel wall-clock run time respectively, N_{proc} is the number of processors used for the simulation, m_s is the total memory used for the serial run and m_{proc} is the total memory of processor number $proc$ of the parallel run.

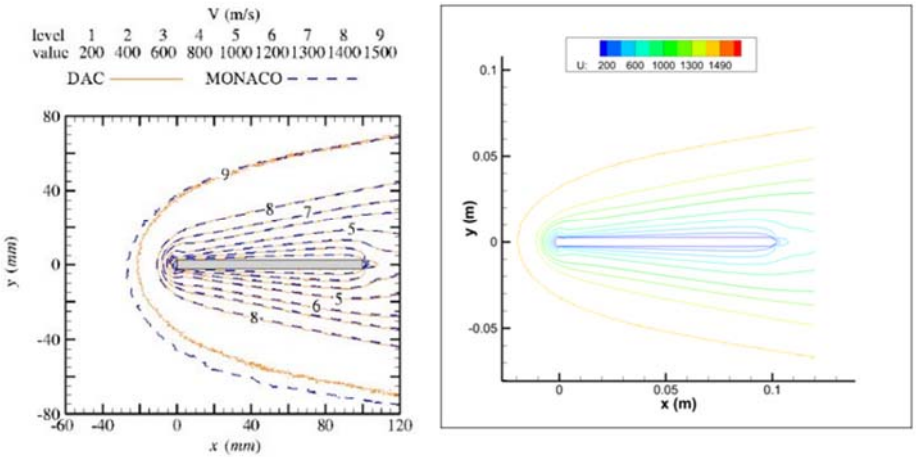

Figure 3. Velocity contours. Right: SPARTA results (flat plate test case).

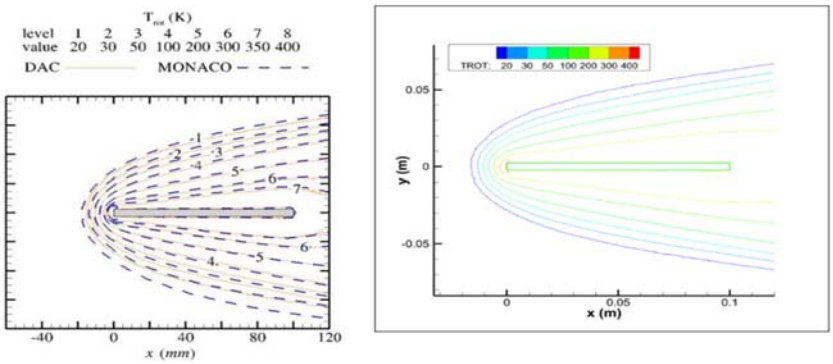

Figure 4. Rotational Temperature contours. Right: SPARTA results (flat plate test case).

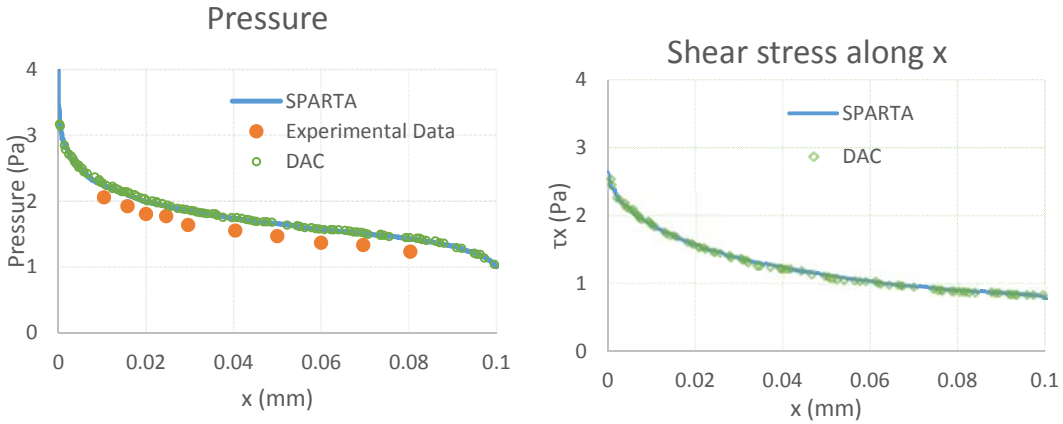

Figure 5. (Left) Pressure along the upper surface, (Right) shear stress along x-axis (flat plate test case).

From the corresponding plots it can be observed that for this case DAC has a better parallel efficiency than SPARTA, but it has to be mentioned that the number of particles used was not very large. Regarding the second parameter, SPARTA shows a remarkable memory spread, using almost the same memory for the serial and the parallel runs. Every time we doubled the number of processors SPARTA needed just 3 additional megabytes of memory, compared to the previous run, with the exception of the 16 and 32 processors, where the 32 processors run required 30 megabytes more than the 16 processors one. Although for this test case DAC software demonstrated a better scale-up compared to SPARTA, the latter requires much less memory storage.

Figures 3, 4 illustrate the results of the flow field contours. A qualitative comparison between the current results and the reference ones shows a good agreement between the simulated flow fields. Moreover, the boundary layer around the flat plate, located at about $0 < x < 100\ mm$, and the oblique diffuse shock are similarly predicted. Comparable results are also observed for the rotational temperature contours.

Figures 5, 6 represent the DAC and SPARTA results of pressure, shear stress, and heat flux along the plate's upper surface; regarding pressure and heat flux, experimental results provided in [12] are included. As it can be observed, there is a very good agreement between DAC and SPARTA in the pressure distribution along the upper surface of the flat plate. For the shear stress distribution along the *x*-axis it can be observed that both codes produce very smooth and similar results. However, a difference can be observed in the heat flux results, where SPARTA is in better agreement with the available experimental ones, compared to DAC.

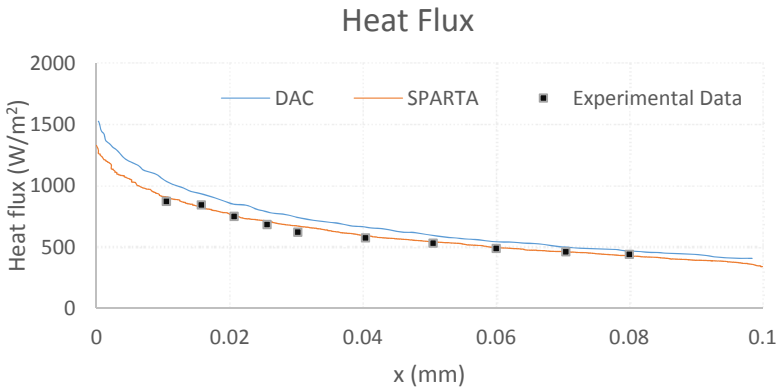

Figure 6. Heat flux on the upper surface (flat plate test case).

3.2 70-degree planetary probe

In this test case a test model proposed by the AGARD Group was used. The model is a 70-degree blunt cone mounted on a stick, as presented in figure 7. The forebody of the model is identical to that of the mars pathfinder reentry vehicle. Experimental results from the SR3 low-density wind tunnel were obtained from [13, 14]; the density flowfields, drag coefficients, and surface heat transfer were measured. In this test case two different grids were used: one Cartesian uniform grid with 600 cells in the *x*-axis and 600 cells in the *r*-axis, and a two level Cartesian grid with a refinement of 10 by 10 cells along the cone's body. The experimental flow conditions and the experimental results are contained in Tables 3 and 4 respectively, whereas the simulation flowfield parameters are shown in Table 2. Due to the symmetry of the problem the flow was modelled as a 2d-axisymmetric one.

V_x(m/s)	T_∞ (K)	n_∞	T_w (K)	Time step (s)	Fnum
1502	13.3	3.869×10^{20}	300	1.3×10^{-7}	7.2×10^{16}

Table 2: 70-degree planetary probe simulation properties.

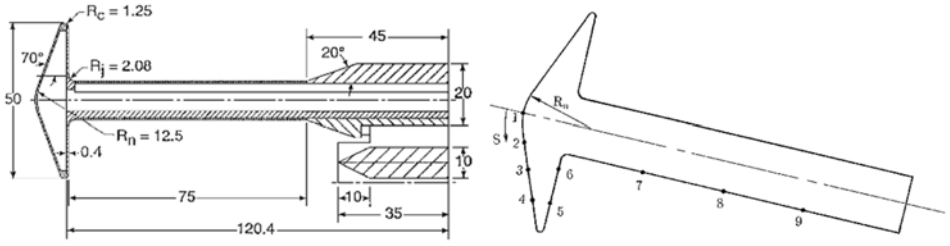

Figure 7. (Left) Planetary probe geometry [13]. (Right) Thermocouple positions [13].

Flow cond.	Gas	$Mach$	T_0, K	$p_0, bars$	Re_d	$\bar{V}$
1	N_2	20.2	1,100	3.5	1,420	0.53
2	N_2	20	1,100	10	4,175	0.31
3	N_2	20.5	1,300	120	36,265	0.11

Table 3: SR3 wind tunnel experimental test conditions [13].

In this work only the first set of flow conditions was simulated, due to the lowest flowfield density in comparison to the other two sets. Moreover, the test model is perpendicular to the free flow, having a 0-degree angle of attack. In Table 5 the results of the heat transfer on the surface of the model, obtained using the uniform and the refined grid, are summarized. Furthermore, figure 8 contains a comparison between the results computed by SPARTA and experimental ones [13] for the specific flow conditions.

		$q, kW/m^2$			
Thermocouple	S/R_n	$a = 0\ deg$	$a = 10\ deg$	$a = 20\ deg$	$a = 30\ deg$
1	0	10.23	9.89	7.59	6.60
2	0.52	8.39	8.07	6.78	5.81
3	1.04	6.33	6.93	6.93	5.72
4	1.56	5.12	6.63	7.53	7.23
5	2.68	<0.02	<0.02	<0.02	<0.02
6	3.32	<0.02	<0.02	<0.02	<0.02
7	5.06	0.13	0.20	0.33	0.59
8	6.50	0.33	0.46	1.22	2.04
9	7.94	0.43	0.82	1.58	2.70

Table 4: Experimental heating rates for the "flow conditions 1" subcase [13] (70-degree planetary probe case).

Uniform grid (kW/m^2)	Refined grid (kW/m^2)
10.2281	10.382
8.39273	8.51419
6.97913	7.122774
6.62745	6.55766
0.002435	0.00251879
0.002079	0.00210614
0.115016	0.101322
0.284723	0.305997
0.363092	0.372261

Table 5: Comparison between uniform and refined grid results (70-degree planetary probe case).

As it can be observed from figures 9 and 10, there is a separation region behind the cone; a small vortex develops at the back of the cone. The vortex seems to be stable but lacks of resolution, due to the rarefaction of the flow field behind the cone. For the same reason, as shown in Table 4, the thermocouples' readings were not accurate enough in the corresponding positions. Generally, the physics of the flow have been captured adequately by SPARTA, for the utilized discretization grids.

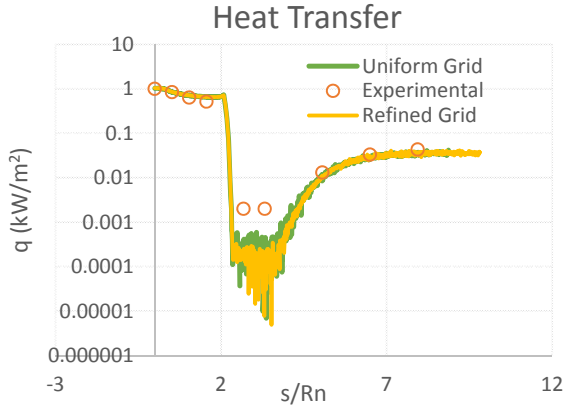

Figure 8. Surface heat transfer results (70-degree planetary probe case).

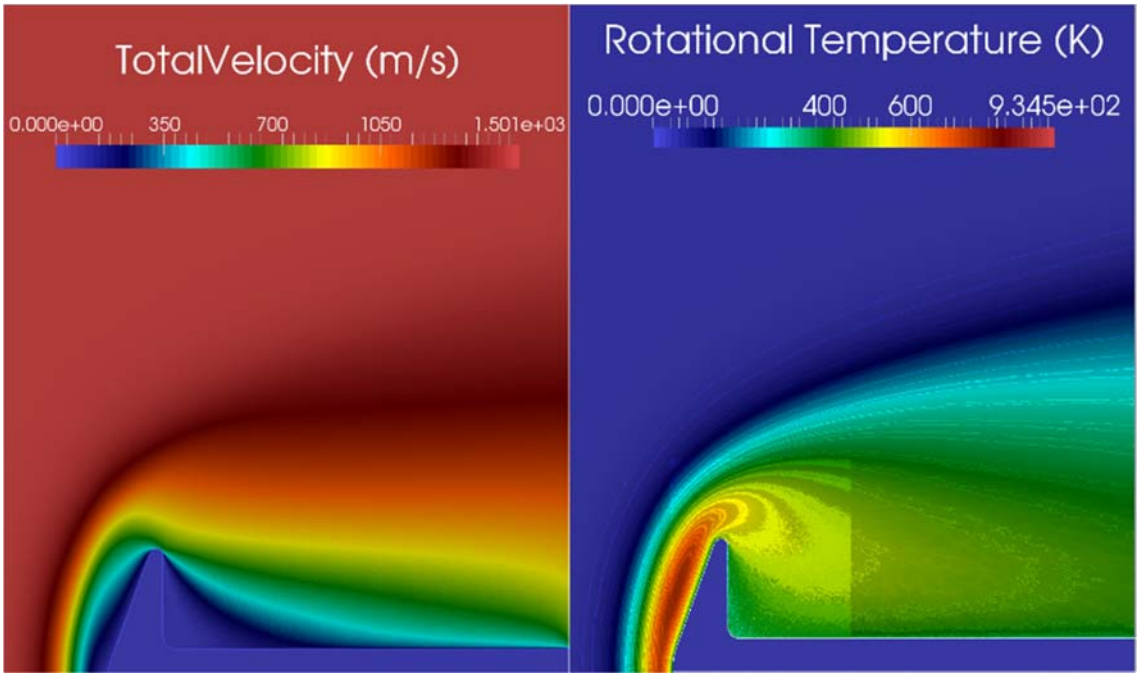

Figure 9. (Left) Total velocity contours. (Right) Total temperature contours (70-degree planetary probe case).

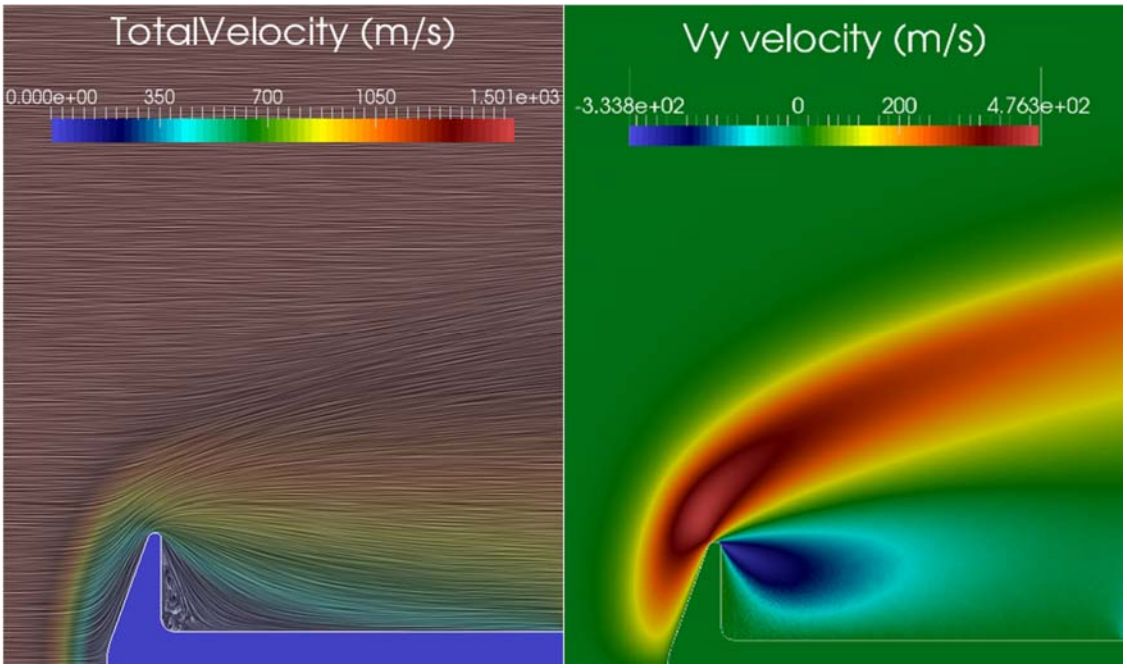

Figure 10. (Left) Oil flow lined around the cone. (Right) Velocity along the *y*-axis. (70-degree planetary probe case).

3.3 A Mach 15.6 flow over a flared cylinder

The last test case included in this study is the CUBRC Run 11 test case [17]; the heat transfer and pressure distributions along a flared cylinder's surface were studied. The reason for including this test case was that it has been extensively studied in the open literature with both DSMC and CFD methods. In order to capture the complex flow in this test case, first we had to identify the size of the grid cells, as well as the refinement regions, and then the related computational parameters, such as the appropriate time-step, the time needed for the flow to develop and finally the number of the samples needed for computing accurate enough results. Although two different sets of flow conditions are available for the CUBRC experiment, only the 48-inch Run 7 was considered in this work.

The flow conditions for both sets are contained in Table 6. The computational domain for this study is from -0.001m to 0.22m in the *x*-axis and from 0m to 0.12m in the *r*-axis. The grid used contains 957 cells along the *x*-axis and 440 cells along the *r*-axis, while there is a refined area from cell 347 till 957 in the *x*-axis and from cell 1 till 440 in the *r*-axis. In the refined area each cell of the initial grid is divided in 10 by 10 sub cells. The time step used in this simulation was equal to $2.0\text{x}10^{-8}\ sec$; it was selected so that each particle to need more than 3 time steps to cross a coarse grid cell. The flow evolved for 246,000 steps and was sampled for another 12,000.

In this test case the results obtained are compared to the experimental ones and to simulation results computed by Moss and Bird using the DS2V solver [17]. Table 6 summarizes the flow conditions for this test case, while Table 7 contains the parameters used for this simulation; figure 11(Left) presents the geometry of the cylinder as obtained from [17], while figure 11(Right) contains the computed result for the pressure on the upper surface of the cylinder and the heat transfer by the DS2V code [17]. This test case was also modelled in this work as a 2d-axisymmetric one.

Run	$V_\infty, m/s$	n_∞, m^{-3}	$T_{\infty,T}, K$	$\rho_\infty, kg/m^3$	$p_\infty, N/m^2$	M_∞	Re_∞, m^{-1}	Gas
48-Inch Run 7	2073	3.779×10^{21}	42.6	1.757×10^{-4}	2.23	15.6	1.37467×10^5	N_2
LENS Run 11	2484	1.197×10^{22}	95.6	5.566×10^{-4}	15.86	12.4	2.08333×10^5	N_2

Table 6. Flow conditions sets obtained from [17] (flared cylinder case).

V_x(m/s)	T_∞ (K)	n_∞	T_w (K)	Time step (s)	Fnum
2484	95.6	1.197×10^{22}	293	$2.0e^{-8}$	$4.4 \times e^{18}$

Table 7. Computational parameters used in the simulations (flared cylinder case).

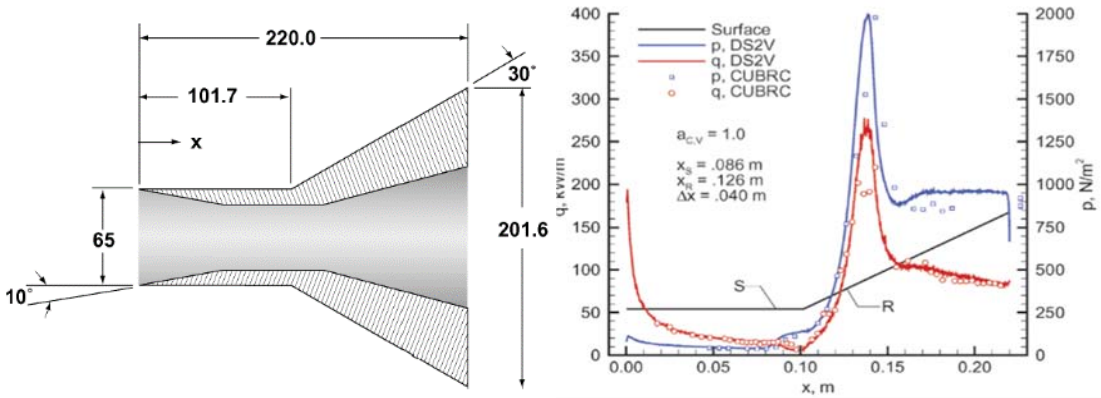

Figure 11. (Left) Flared cylinder geometry (units in millimeters) [17].
(Right) Computed pressure and heat transfer by DS2V [17].

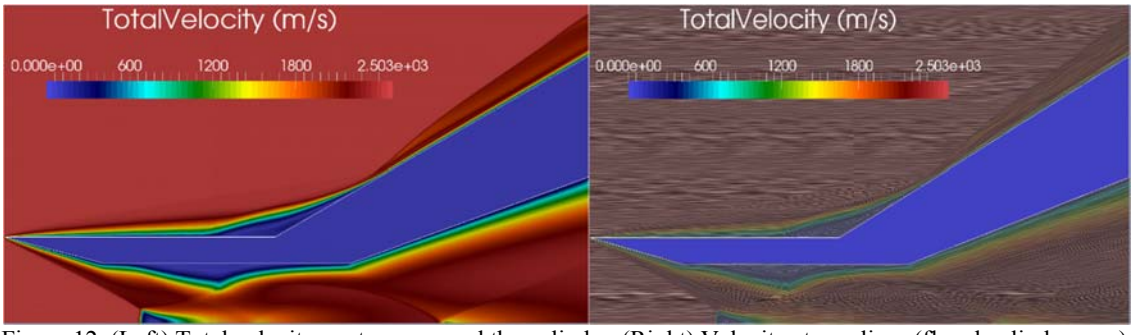

Figure 12. (Left) Total velocity contours around the cylinder. (Right) Velocity streamlines (flared cylinder case).

Figure 12(Left) contains the total velocity distribution across the flared cylinder, as computed by SPARTA. A barrel shock can be observed at the internal area of the cylinder, which results in the creation of a small Mach disk. Moreover, at the external surface a separation of the flow in the region around the cylinder's flare is evident. Furthermore, two vortices are formed, one at the separation area on the external surface and one at the internal surface of the cylinder. In figure 13 the results of the computed heat transfer and pressure on the external surface,

compared to experimental data, are presented. The simulation results have been obtained with three different grids: two uniform ones (with 2 million and 10 million particles) and the refined one. It can be observed that all grids (both uniforms and the refined one) capture heat transfer and pressure quite well from the cylinder's bevel edge till the start of the flare. In the area around the flare all grids simulate heat transfer adequately enough. However, as we move forward on the cylinder's upper surface and we are approaching the shock reattachment region, the uniform grids compute an unphysical heat peak. Moreover, for pressure computation the uniform grids provide an accurate result in the area around the external vortex whereas the refined grid over-predicts pressure distribution. Nevertheless, the refined grid predicts pressure more accurately than the uniform grids in the shock reattachment region. It should be noted here that it has not been examined the behavior of the uniform grid in the addition of a large number of particles while keeping the same number of particles in the refined grid. However, the presented results emphasize the importance of the proper grid refinement in regions with steep gradients of the flow quantities, to considerably improve the simulation results.

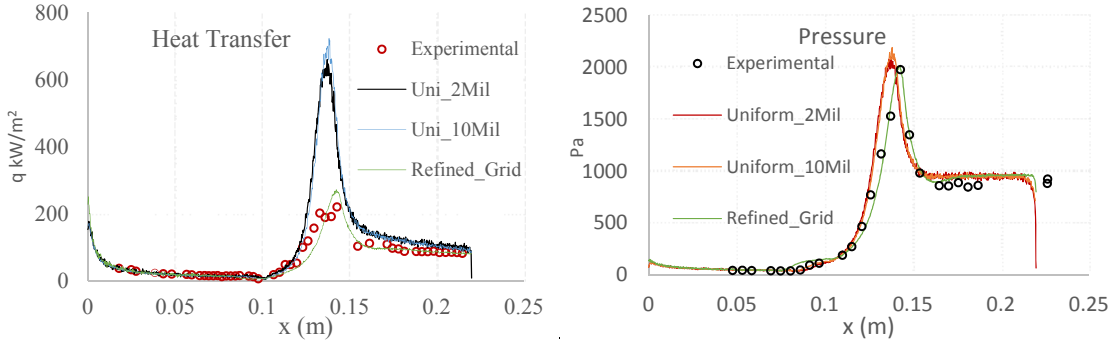

Figure 13. (Left) Heat transfer on the external surface of the cylinder. (Right) Pressure distribution on the external surface of the cylinder (flared cylinder case).

4 CONCLUSIONS

In this study 3 hypersonic flow test cases have been considered for the assessment of an open-source, parallel DSMC code, named SPARTA: α 2d flow around a flat plate, and two 2d-axisymmetric flows, one around a 70-degree blunt cone and one around a flared cylinder. For the first two cases the application of the DSMC method was not computationally intensive, whereas in the case of the flared cylinder, where large separation regions and shock interactions exist, the numerical simulation was computationally demanding.

The simulation results demonstrated that SPARTA code is capable of predicting accurately such complicated and demanding flows; it should be emphasized that for the flared cylinder case the flow is almost in the near-continuum regime. In order to obtain accurate results a careful study of the grid size, along with the construction of grid-refined areas in positions with steep gradients of the flow quantities are needed, before the beginning of the simulation. Despite the large computational resources needed for such simulations, very good agreement between the simulation and the experimental results has been achieved for all the cases considered. Finally, it has to be mentioned that SPARTA code reproduced correctly and accurately all the complicated details of the considered flows, such as shock interactions and vortex formation. The general availability of more powerful computers will certainly further expand the applicability of the DSMC methodology to model the computationally demanding near-continuum flows.

ACKNOWLEDGEMENTS

This work has been co-funded by the European Commission (European Regional Development Fund) and by the Greek State, through the Operational Programme "Competitiveness and Entrepreneurship (OPCE II 2007-2013), National Strategic Reference Framework - Research funded project: "Development of a spark discharge aerosol nanoparticle generator for gas flow visualisation and for fubrication of nanostructured materials for gas sensing applications – DE_SPARK_NANO_GEN", 11SYN_5_144, in the framework of the Action "COOPERATION 2011" – Partnerships of Production and Research Institutions in Focused Research and Technology Sectors.

REFERENCES

[1] Gallis, M. A., Torczynski, J. R., Plimpton, S. J., Rader, D.J., Koehler, T. (2014), "Direct Simulation Monte Carlo: The Quest for Speed", *Proceedings of the 29th Rarefied Gas Dynamic (RGD) Symposium,* Xi'an, China, July 2014.

[2] Bird, G.A (1994), "*Molecular Gas Dynamics and the Direct Simulation of Gas Flows*", Oxford Engineering Series.

[3] LeBeau, G.J (1999), "A parallel implementation of the direct simulation Monte Carlo method", *Journal of Computer Methods in Applied Mechanics and Engineering*, Vol. 174, pp 319-337.

[4] Ivanov, M.S., Markelov, G.N., Gimelshein, S.F. (1998), "Statistical Simulation of Reactive Rarefied Flows: Numerical Approach and Applications", *Proceedings of the 7th AIAA/ASME Joint Thermophysics and Heat Transfer Conference*, Albuquerque, June 1998, AIAA Paper 98-2669.

[5] Dietrich, S., Boyd, I.D. (1996), "Scalar and parallel implementation of the direct simulation monte carlo method", *Journal of Computational Physics,* Vol. 126, pp 328-342.

[6] Bartel, T.J., Plimpton, S.J., Gallis, M.A. (2001), "*A 2-D Direct Simulation Monte Carlo (DSMC) Code for Multi-Processor Computers*", Sandia National Laboratories Technical Report, 2001-2901, Albuquerque.

[7] Gao, D., Schwartzentruber, T.E. (2011), "Optimizations and OpenMP implementation for the direct simulation Monte Carlo method", *Computers & Fluids,* Vol. 42, pp 73-81.

[8] Scanlon, T.J., Roochi, E., White, C., Darbandi, M., Reese, J.M. (2010), "An open-source parallel DSMC code for rarefied gas flows in arbitrary geometries", *Journal of Computers & Fluids*, Vol. 39, pp 2078-2089.

[9] Ahmad, A.O. (2011), "Capturing Shock Waves Using an Open-Source, Direct Simulation Monte Carlo (DSMC) Code", *Paper presented at 4th European Conference for Aero-Space Sciences (EUCASS),* St. Petersburg, Russian Federation 4-8 July 2011.

[10] Moss, J.N., LeBeau, G.J., Glass C.E. (2002), "Hypersonic Shock Interactions About a 25º / 65º Sharp Cone", NASA technical report, TM-2002-211778, Springfield.

[11] Boyd, I.D. (2009), "*Direct Simulation Monte Carlo for Atmospheric Entry. 2. Code Development and Application Results*", Michigan University Ann Arbor report, Michigan.

[12] Allègre, J., Raffin, M., Chpoun, A., Gottesdiener, L. (1992), "Rarefied Hypersonic Flow over a Flat Plate with Tuncated Leading Edge", *Progress in Astronautics and Aeronautics,* pp. 285-295.

[13] Allègre, J., Bisch, D., Lengrand, J. C. (1997), "Experimental Rarefied Heat Transfer at Hypersonic Conditions over a 70-Degree Blunted Cone", *Journal of Spacecraft and Rockets,* Vol. 34, No. 6, pp. 724-728.

[14] Allègre, J., Bisch, D., Lengrand, J.C. (1997), "Experimental Rarefied Density Flowfields at Hypersonic Conditions over a 70-Degree Blunted Cone", Journal of Spacecraft and Rockets, Vol. 34, No. 6, pp. 714-718.

[15] Harvey, J.K., "A Review of a Validation Exercise on the use of the DSMC Method to Compute Viscous/Inviscid Interactions in Hypersonic Flow", *Proceedings of the 36th AIAA Thermophysics Conference,* Orlando, 23-26 June 2003.

[16] Padilla, J. F. (2010), "Comparison of DAC and MONACO Codes with Flat Plate Simulation", *Technical Report,* No. 20100029686 .

[17] Moss, J.N., Bird, G.A. (2005), "Direct Simulation Monte Carlo Simulations of Hypersonic Flows with shock interactions", *AIAA Journal,* Vol. 43, No. 12, pp. 2565-2573.